DRAFT VERSION APRIL 14, 2020
Typeset using LaTeX **twocolumn** style in AASTeX62

Against the Planetary Interpretation of PTFO 8-8695b

L. G. BOUMA[1] AND J. N. WINN[1]

[1] *Department of Astrophysical Sciences, Princeton University, 4 Ivy Lane, Princeton, NJ 08540, USA*

(Received April 14, 2020; Revised —; Accepted —)

Submitted to AAS journals.

ABSTRACT

PTFO 8-8695b could be the youngest, shortest-period hot Jupiter known. However it has not been shown to be a planet. TESS recently observed PTFO 8-8695 for one month. The TESS lightcurve shows that the dominant variability in this system is a sinusoidal modulation with a "long" period P_ℓ of 11.96 hours, likely caused by stellar rotation. Also present is a complex signal, previously identified as the planet candidate, that repeats with a "short" period P_s of 10.74 hours. The "long" and "short" signals show the expected beat every 4.48 days. There is a dip in the complex, short-period signal. However ground-based photometry from the past decade shows that the orbital phase of the dip seems to have instantaneously jumped, at least once, and maybe twice. The TESS epoch of the dip is consistent with recent observations by Tanimoto et al., and differs from the discovery epoch by 5.14 hours. Planets do not "jump" in orbital phase. Given the available evidence, PTFO 8-8695 seems consistent with the "transient dipping" phenomenology observed in many young M dwarfs. It seems rather unlikely to be a planet.

1. INTRODUCTION

If PTFO 8-8695b were a planet, it would be exceptional. A transiting hot Jupiter, orbiting a ≈3 Myr old M dwarf in ORION would make it the youngest hot Jupiter known. Its orbital period of only 12 HOURS would also make it the shortest period hot Jupiter known.

2. THE DATA

2.1. *Observations*

PTFO 8-8695 was observed by TESS with Camera 1, CCD 1, from December 15, 2018 to January 6, 2019, during the sixth sector of science operations. The star was designated TIC 264461976 in the TESS Input Catalog (Stassun et al. 2018, 2019). The pixel data for an 11×11 array surrounding PTFO 8-8695 were averaged into 2-minute stacks by the onboard computer. Each 2048×2048 image from the CCD was also averaged into 30-minute stacks, and saved as a "full frame image" (FFI).

The 2-minute stacks for PTFO 8-8695 were then reduced to lightcurves by the Science Processing Operations Center (SPOC) at NASA Ames (Jenkins et al. 2016). Our main analysis used the resulting Presearch Data Conditioning (PDC) lightcurve. The PDC lightcurve aperture used pixels chosen to maximize the SNR of the total flux of the target (Smith et al. 2017a). Non-astrophysical variability was removed through the methods discussed by Smith et al. (2017b).

Corresponding author: L. G. Bouma
luke@astro.princeton.edu

As an independent check on the shorter cadence SPOC light-curve, we separately processed the 30-minute image stacks as part of the Cluster Difference Imaging Photometric Survey (CDIPS; (Bouma et al. 2019)). The CDIPS lightcurve used a circular aperture with radius 1 pixel.

To clean the data, we removed all points with non-zero quality flags (*e.g.*, Tenenbaum & Jenkins 2018). We also masked out the first and last 6 hours of each orbit, since there is often systematic red noise during those times. Both the CDIPS and PDC lightcurves showed a clear discontinuous "jump" in the last few days of orbit 20, which seemed likely to be an instrumental systematic. We correspondingly masked out times from BJD 2458488.3 until the end of the orbit. The PDC lightcurve initially had 15,678 points. The quality cut removed 854 points, masking the orbit edges removed an additional 716, and removing the final few days of orbit 20 removed an additional 1079. After cleaning, 83% of the initial flux measurements remained.

We normalized these points by dividing out the median flux. We then subtracted by unity to simplify subsequent analysis. Many of these and subsequent processing steps were performed using `astrobase` (Bhatti et al. 2018).

2.2. *Visual Inspection*

Our initial inspection of the lightcurve, in both its 2-minute PDCSAP and 30-minute FFI forms, showed a strong sinusoidal beat signal (Figure 1, top panel).

As a precursor to more detailed analysis, we calculated generalized Lomb-Scargle periodograms using `astrobase` (Lomb 1976; Scargle 1982; VanderPlas & Ivezić 2015; Bhatti et al. 2018). The two largest peaks in the Lomb-Scargle peri-

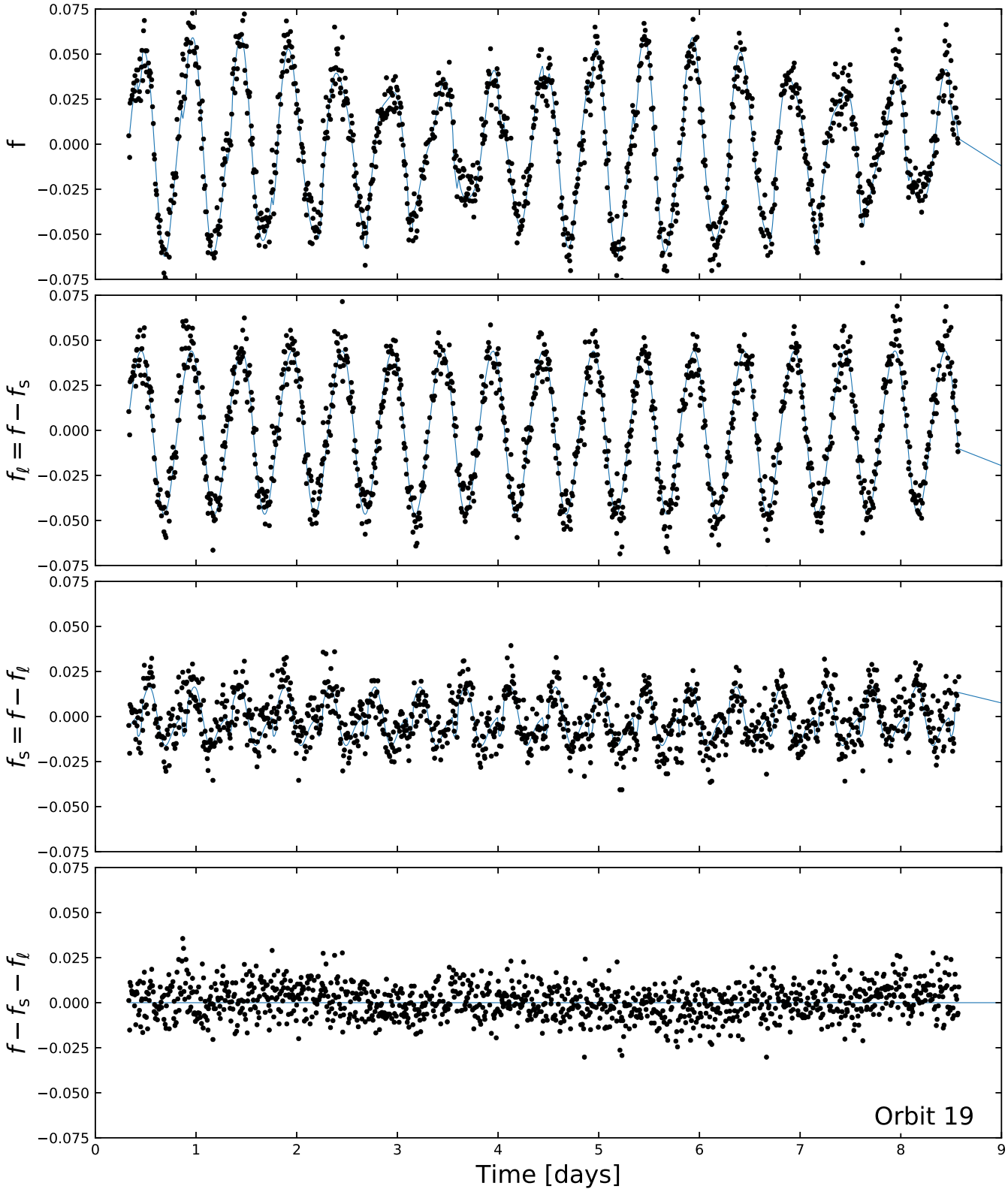

Figure 1. TESS lightcurve of PTFO 8-8695 (Sector 6, Orbit 19). *Top*: "Raw" `PDCSAP` mean-subtracted relative flux versus time. The beat period of 4.48 days is visible by eye. The model plotted underneath the data includes 2 harmonics at the long period P_ℓ, plus 2 harmonics and a transit at the short period P_s. *Upper middle*: Long-period signal, equal to the raw signal minus the short-period signal. *Lower middle*: Short-period signal, equal to the raw signal minus the long-period signal. *Bottom*: residual. The data are binned from 2 to 10 minute cadence as a convenience for plotting and fitting.

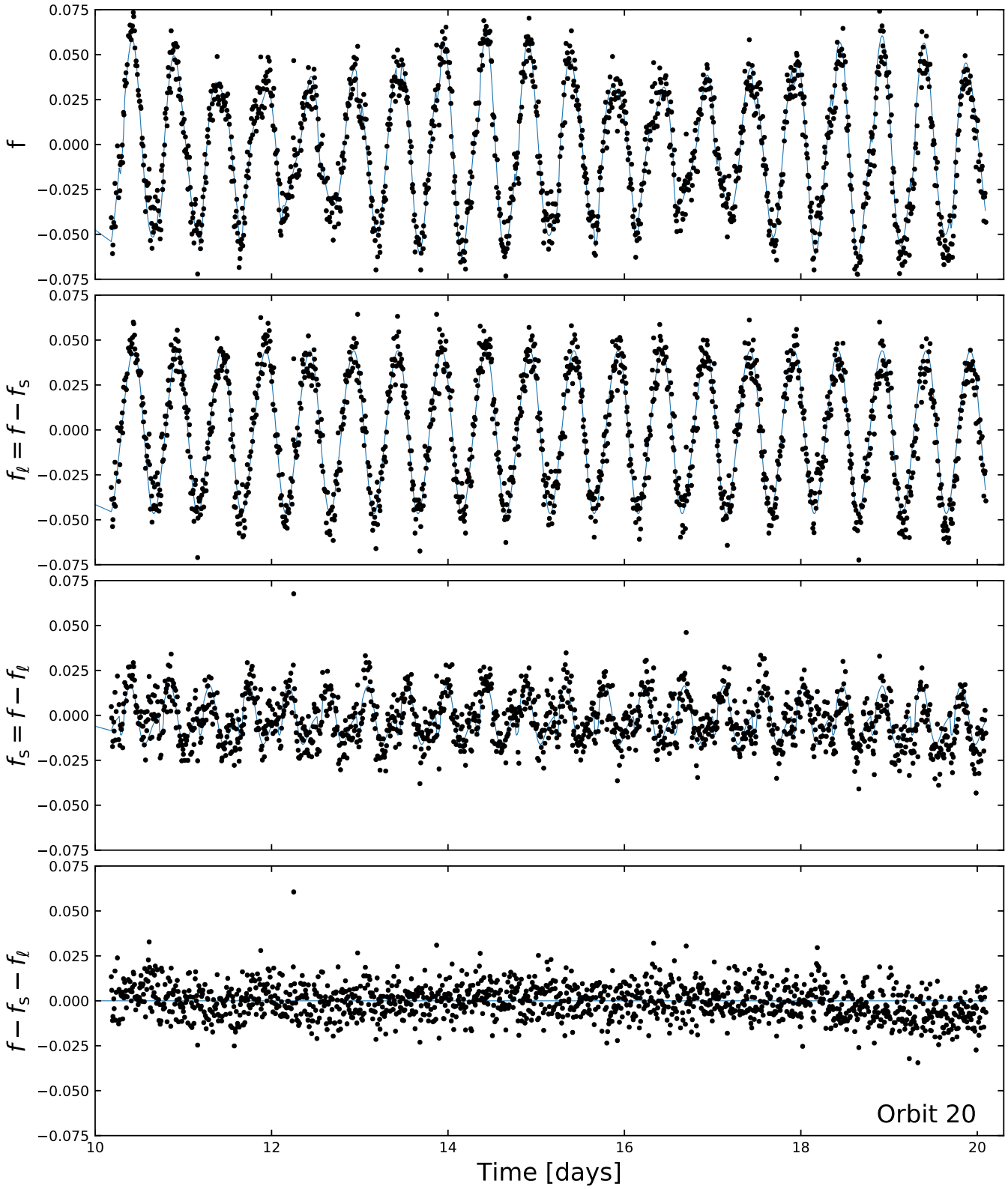

Figure 2. TESS lightcurve of PTFO 8-8695 (Sector 6, Orbit 20). Panels are as in Figure 1.

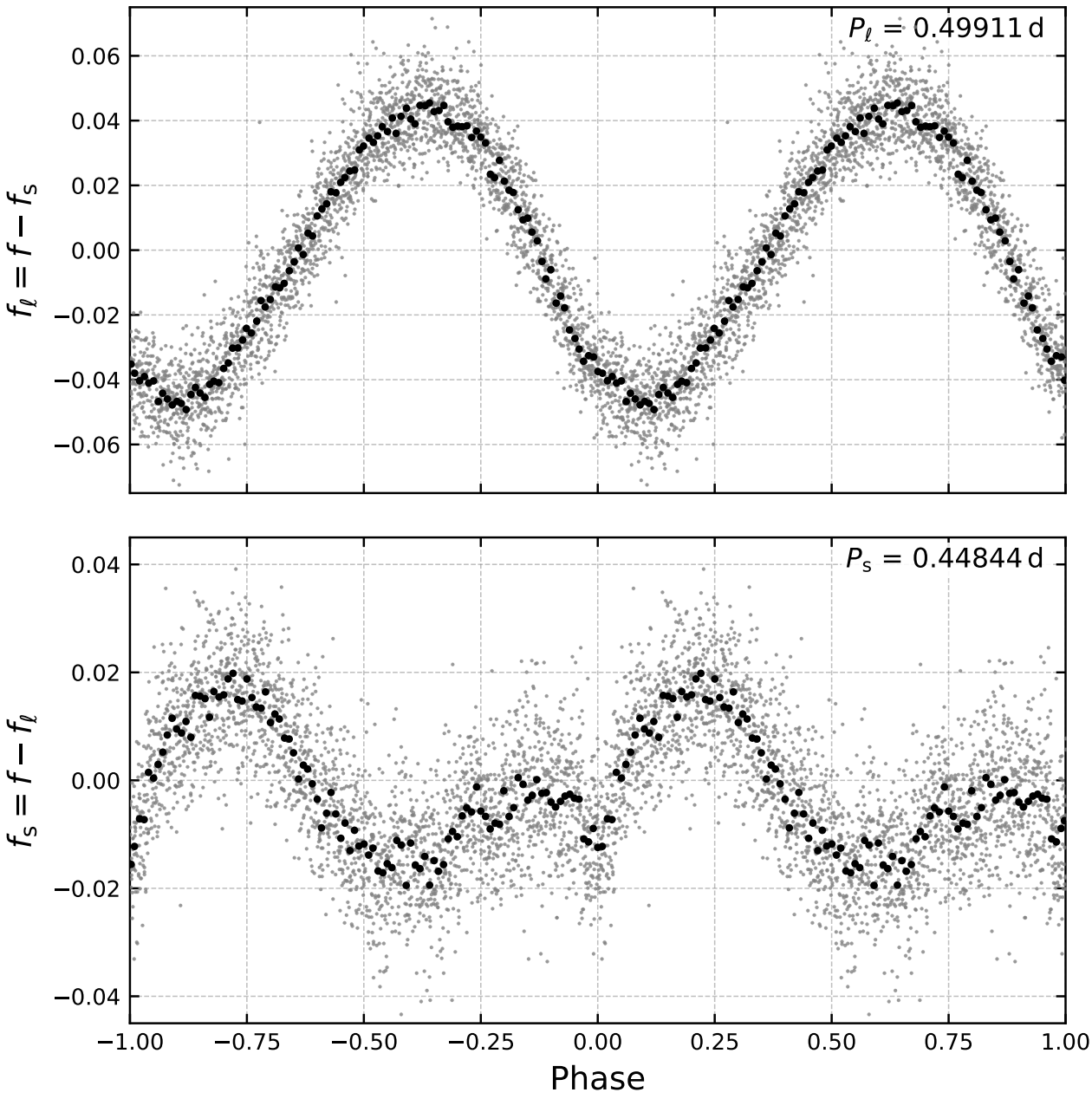

Figure 3. Phase-folded long and short-period signals. *Top*: Long-period signal, as in Figure 1. *Bottom*: Short-period signal. The reference phase is set to the "planetary" dip. Gray points are the 10 minute cadence `PDCSAP` flux. Black points are binned to 100 points per period.

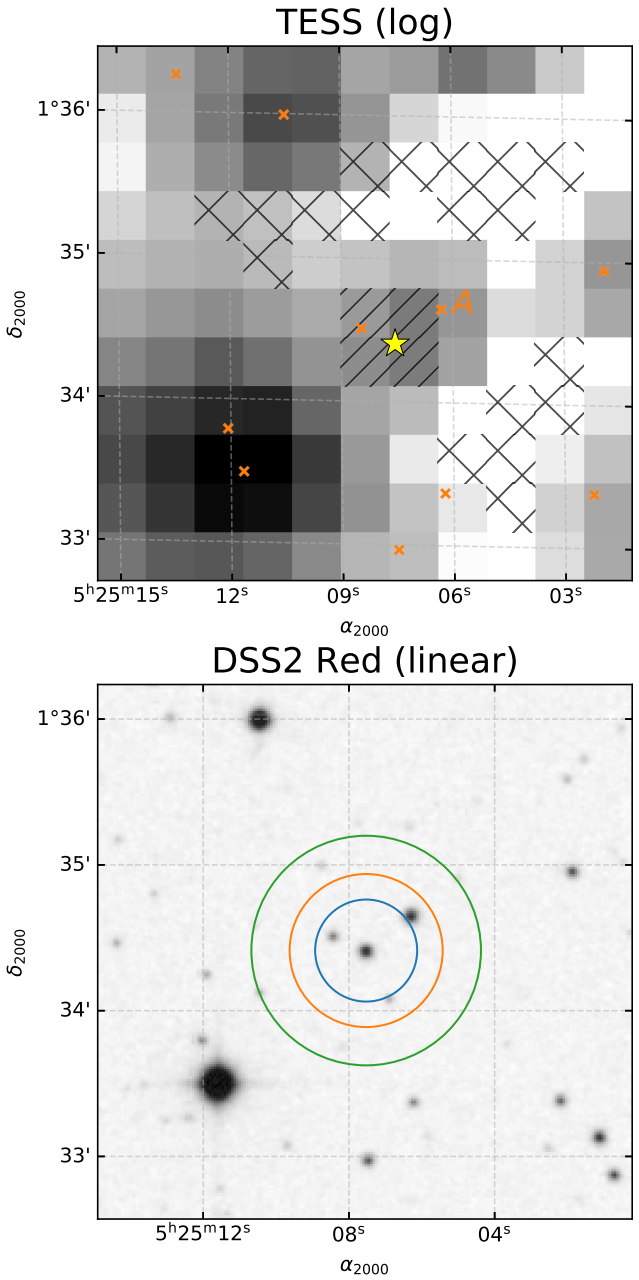

Figure 4. Scene used for blend analysis. *Top:* Mean TESS image of PTFO 8-8695 over Sector 6, with a log-stretch. The position of PTFO 8-8695 is shown with a yellow star. Neighbors with $T < 17$ are shown with orange crosses. The apertures used to measure the background and target star flux are shown with X and / hatches, respectively. *Bottom:* Digitized Sky Survey *R*-band image of the same field, with a linear stretch. The circles show apertures of radii 1, 1.5, and 2.25 pixels used in part of our blend analysis. The pixel level TESS data show that "Star A" does not contribute variability at either of the two observed periods (see Section 3.3).

odogram of the lightcurve were clearly separated at a "short" period $P_s \approx 0.448$ days and a "long" period $P_\ell \approx 0.499$ days. The P_ℓ peak had the greater power of the two. Smaller harmonics from each of these two dominants peaks were also present.

The peak-to-peak amplitude at maximum, when the two signals constructively interfere, is about 14%. At minimum, the peak-to-peak amplitude is about 6%. Assuming the signals are just two sinusoids, algebra tells us that the peak-to-peak amplitudes should therefore be 10% for the long-period signal, and 4% for the short-period signal. These order-of-magnitude numbers will turn out to be roughly correct.

Initial signal-processing experiments fitting out splines or sinusoids showed that after subtracting out the long-period signal, the short-period signal dominated the periodogram, and vice-versa. However it quickly became clear that it would be beneficial to simultaneously model the signals separately, in order to preserve the power at each frequency.

3. THE MODEL

3.1. *Model Description*

We opted to model the lightcurve as a linear combination of Fourier harmonics at the short and long periods, plus a transit at the short period. Symbolically, the total flux f is given as

$$f = f_s + f_\ell = f_{\text{transit,s}} + f_{\text{Fourier,s}} + f_{\text{Fourier},\ell}, \tag{1}$$

where f_s is the relative flux at the short period, and f_ℓ is the flux at the long period. Writing out the Fourier terms,

$$\begin{aligned} f = & f_{\text{transit,s}} + \sum_{n=1}^{N} A_n \sin(n\omega_s t) + \sum_{n=1}^{N} B_n \cos(n\omega_s t) \\ & + \sum_{m=1}^{M} A_m \sin(m[\omega_\ell t + \phi_\ell]) + \sum_{m=1}^{M} B_m \cos(m[\omega_\ell t + \phi_\ell]), \end{aligned} \tag{2}$$

for N and M the total number of harmonics at the short and long periods, respectively, A_i and B_i the amplitudes for each harmonic term (potentially negative), and $\omega_i = 2\pi/P_i$ the angular frequency for i the short or long period index. We fixed the "phase-offset" for the short period signal to be zero, and let the reference time for the long period signal float by introducing ϕ_ℓ. Since we did not a priori know how many harmonics would be appropriate, we considered a number of different choices for N and M, and used the Bayesian information criterion to choose the appropriate model (Table 1).

As an example, one possible model could be a transit, plus $N = 2$ harmonics of sines and cosines at the short period, plus $M = 1$ harmonics at the long period. In this case, the free parameters would be as follows. For the transit, we would fit for the impact parameter, the planet-to-star radius ratio, two quadratic limb darkening parameters, the planet orbital period (equal to the short period), the reference time for the transit, and the mean flux. There would be $2N = 4$ additional Fourier amplitudes at the short period, plus $2M = 2$ Fourier amplitudes at the long period, and well as the long period itself and its phase. For this case, we therefore fitted 14 free parameters.

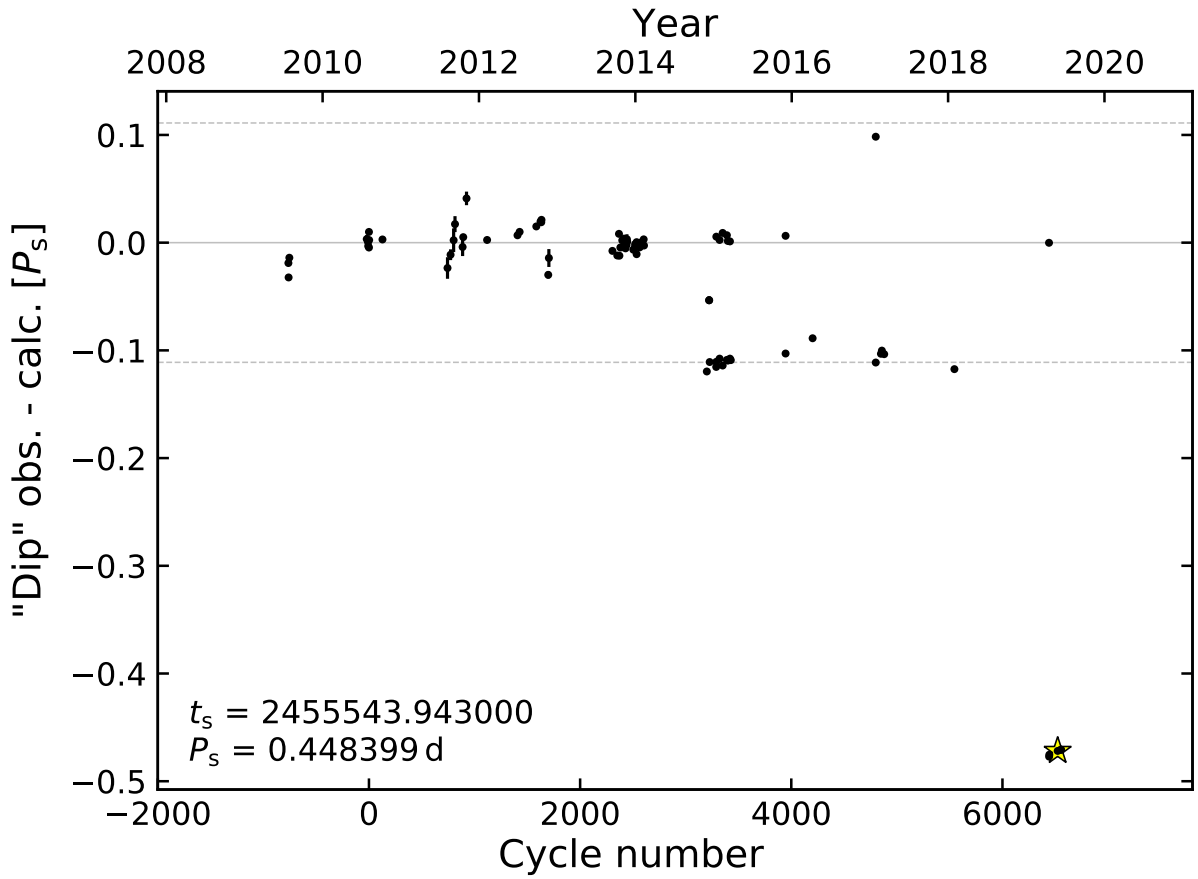

Figure 5. Timing residuals for PTFO 8-8695b from a decade of monitoring. Black points are times of "dips", minus the indicated linear ephemeris. The y-axis is given in units of phase for the short-period signal. The star shows the binned TESS ephemeris. "Dips" have been observed by van Eyken et al. (2012), Ciardi et al. (2015), Yu et al. (2015), Raetz et al. (2016), Onitsuka et al. (2017), and Tanimoto et al. (2020). Certain dips (*e.g.*, the one at phase 0 in mid-2019) are consistent with noise, and were likely reported because something was *expected*, rather than convincingly *observed*. Horizontal dashed lines are drawn at $\pm(P_\ell - P_s)/P_s$, highlighting what could be either a numerical coincidence or an observational bias. The orbital phase observed by TESS is consistent with that of Tanimoto et al. (2020), and quite different from the original phase.

We implemented and fitted the models using `PyMC3`, which is built on `theano` (Salvatier et al. 2016; Theano Development Team 2016). For the Fourier terms, we used the default math operators. For the exoplanet transit, we used the model and derivatives implemented in `exoplanet` (Foreman-Mackey et al. 2020). Our priors are listed in Table **??**. To speed up the fitting, we binned the cleaned 2 minute lightcurves to 10 minute bins. We correspondingly scaled the uncertainties in the flux measurements by a factor of $\sqrt{5}$. Before sampling, we initialized each model to the maximum a posteriori (MAP) solution. We then sampled using `PyMC3`'s gradient-based No-U-Turn Sampler (Hoffman & Gelman 2014), and used $\hat{R}$ as our convergence diagnostic (Gelman & Rubin 1992). We tested our ability to successfully recover injected parameters using synthetic data, before switching to the actual PTFO 8-8695 lightcurves.

3.2. *Fitting Results*

We considered nine models, with the number of harmonics per frequency N and M ranging from one to three. To select our preferred model, we used the Bayesian information criterion (Table 1). The model with the lowest BIC had two harmonics at the short 11.74 hr period, and two harmonics at the long 11.96 hr period. All of the models have reduced χ^2

Table 1. Model Comparison.

Description	N	M	$N_{\rm data}$	$N_{\rm param}$	χ^2	$\chi^2_{\rm red}$	BIC	ΔBIC
Favored	2	2	2585	17	3523.6	1.372	3657.2	0.0
Somewhat favored	2	3	2585	19	3512.7	1.369	3662.0	4.8
Disfavored	3	2	2585	19	3543.1	1.381	3692.4	35.2
—	3	3	2585	21	3536.8	1.379	3701.9	44.6
—	1	2	2585	15	3680.0	1.432	3797.9	140.7
—	1	3	2585	17	3670.2	1.429	3803.8	146.6
—	2	1	2585	15	3700.9	1.440	3818.8	161.6
—	3	1	2585	17	3710.2	1.445	3843.7	186.5
—	1	1	2585	13	3872.7	1.506	3974.8	317.6

NOTE— N and M are the number of harmonics at the short and long periods, respectively. $N_{\rm data}$ is the number of fitted flux measurements. $N_{\rm param}$ is the number of free parameters in the model. The Bayesian information criterion (BIC) and the difference from the maximum ΔBIC are also listed.

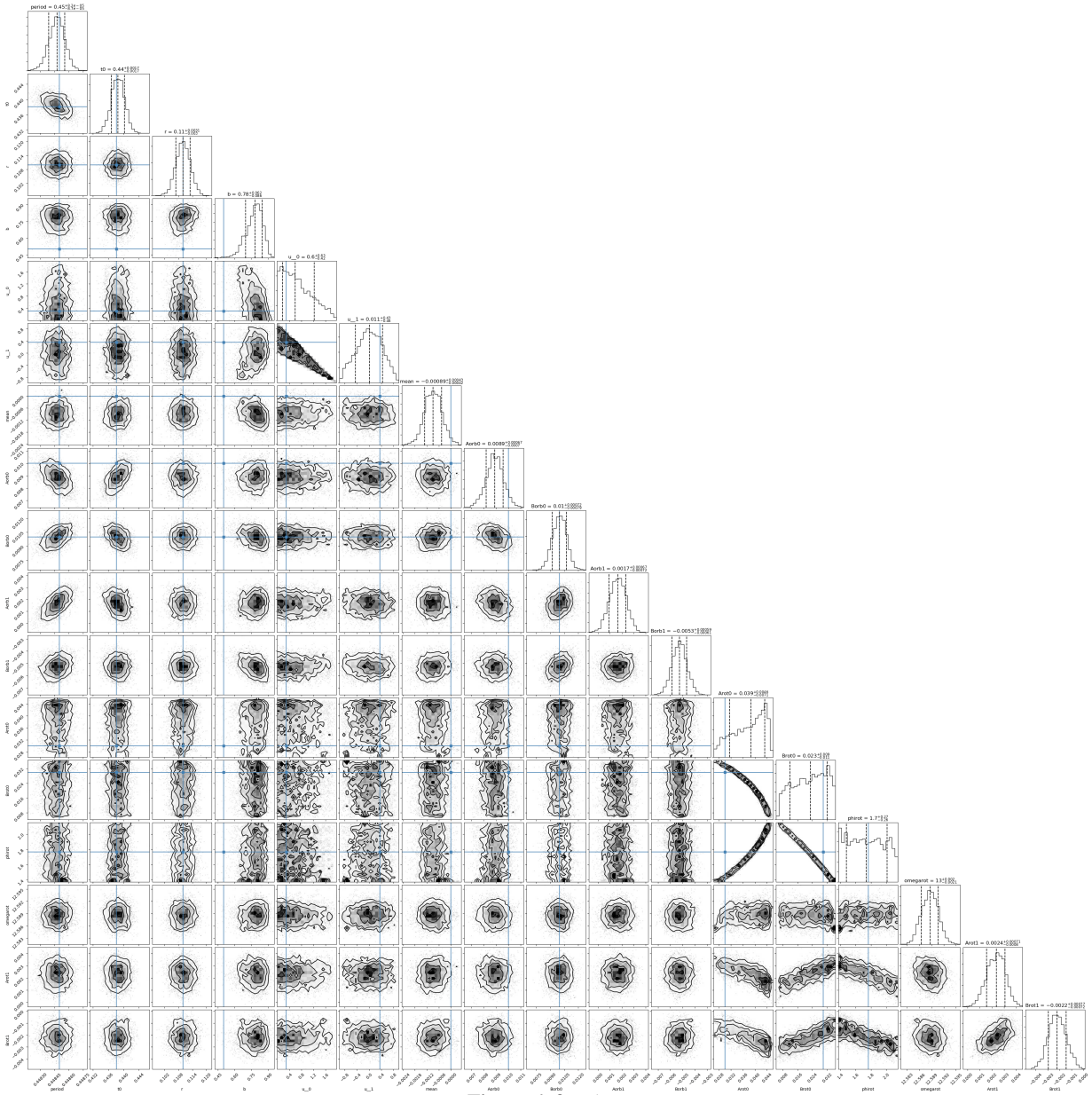

Figure 6. foo. bar

ranging between 1.37 and 1.51, which suggests a plausible, though not perfect agreement between the data and models.

To explore where each model succeeded and failed, we split the raw signal into its respective components (Figures 1 and 2). We also examined the phase-folded signals (Figure 3).

In every model, the variability at the long period is a simple sinusoid with peak-to-peak amplitude ≈10% (Figure 3, top). The variability at the short period is always more complex. A dip of depth ≈1.2%, fit in our model as a transit, lasts ≈0.75 hours. Superposed on the dip is a complex signal with peak-to-peak amplitude of about 4%, which peaks near phase 0.25, and reaches minimum brightness between phases -0.5 and -0.25.

Outside of the primary dip, the short-period signal is relatively smooth, at least from phases 0 to 0.5. However the short-period signal is asymmetric. The flux from phases -0.5 to 0 shows what could be a discontinuous jump, shortly after reaching minimum. This jump was visible in each of the nine models we considered, with different choices for the number of harmonics.

3.3. *Blend considerations*

The TESS pixels are ≈ 21" per side, and so we need to consider whether light from neighboring stars could affect the photometry. The scene is shown in Figure 4. The pixels used to measure the background level are indicated with an 'X' hatch, and the pixels used for the final lightcurve are shown with the '/' hatch.

The target star, PTFO 8-8605 (TIC 264461976), has a T-band magnitude of 14.0, and its position is shown with a star. The other (unlabeled) star inside the target aperture, TIC 264461979, has $T = 16.8$ and so cannot contribute a signal with relative amplitude 10%. The only neighbor that is sufficiently close and bright that its light might contaminate the target star is TIC 264461980, with $T = 14.8$, which we denote "Star A". Star A is 23.6" NW of our target, and based on the magnitude difference could contribute up to 48% the flux of our target star, PTFO 8-8695.

Because PTFO 8-8695 has previously been identified to have periodicity consistent with our measurement of P_s, our main concern regarding blending is the degree to which we can be certain that the long-period signal at P_ℓ also originates from PTFO 8-8695. We took two approaches towards determining the source of the long-period signal.

First, we examined the CDIPS full frame image lightcurves of the target, which are available on MAST (Bouma et al. 2019). The maximal peak-to-peak beat amplitude is consistently $\approx$10% across apertures of radii 1, 1.5, and 2.25 pixels. If Star A were the source of the long-period variability, we would expect the peak variability amplitude to be smallest in the 1 pixel aperture, based on the separation of the sources (Figure 4, bottom). From this test alone, it seems unlikely that Star A is the source of the long-period signal.

Second, we examined the lightcurve of each pixel in the scene individually. We opted to use the interactive tools implemented in `lightkurve` (Lightkurve Collaboration et al. 2018). If Star A were the source of the long-period variability, we would expect the pixels nearest to Star A to show a sinusoidal signal with amplitude exceeding 10%. We find no evidence for this being the case. The pixel directly below Star A does not clearly show the sinusoidal variability, and the peak-to-peak variability in that pixel is $\lesssim 8\%$. In contrast, the south-easternmost pixel within PTFO 8-8695's aperture (the pixel furthest from Star A that was used in the optimal aperture) shows the P_ℓ sinusoidal variability signal at $\approx 10\%$ amplitude.

As there is no evidence in favor of a blend scenario, we conclude that both the P_s and P_ℓ signals originate from PTFO 8-8695.

4. INTERPRETATION

The TESS dip does not phase up where it is supposed to... Figure 5

5. CONCLUSIONS

Software: `astrobase` (Bhatti et al. 2018), `astropy` (Astropy Collaboration et al. 2018), `astroquery` (Ginsburg et al. 2018), `corner` (Foreman-Mackey 2016), `exoplanet` (Agol et al. 2019) `exoplanet` (Foreman-Mackey et al. 2020), and its dependencies (Agol et al. 2019; Kipping 2013; Luger et al. 2019; Theano Development Team 2016). `IPython` (Pérez & Granger 2007), `lightkurve` (Lightkurve Collaboration et al. 2018), `matplotlib` (Hunter 2007), `MESA` (Paxton et al. 2011, 2013, 2015) `numpy` (Walt et al. 2011), `pandas` (McKinney 2010), `PyMC3` (Salvatier et al. 2016), `radvel` (Fulton et al. 2018), `scipy` (Jones et al. 2001).

REFERENCES

Agol, E., Luger, R., & Foreman-Mackey, D. 2019, arXiv e-prints, 1908.03222

Astropy Collaboration, Price-Whelan, A. M., Sipőcz, B. M., et al. 2018, AJ, 156, 123

Bhatti, W., Bouma, L. G., & Wallace, J. 2018, `astrobase`, https://doi.org/10.5281/zenodo.1469822

Bouma, L. G., Hartman, J. D., Bhatti, W., Winn, J. N., & Bakos, G. Á. 2019, ApJS, 245, 13

Ciardi, D. R., Eyken, J. C. v., Barnes, J. W., et al. 2015, The Astrophysical Journal, 809, 42, publisher: IOP Publishing

Foreman-Mackey, D. 2016, The Journal of Open Source Software, 24

Foreman-Mackey, D., Czekala, I., Luger, R., et al. 2020, exoplanet-dev/exoplanet v0.2.6

Fulton, B. J., Petigura, E. A., Blunt, S., & Sinukoff, E. 2018, PASP, 130, 044504

Gelman, A., & Rubin, D. B. 1992, Statistical Science, 7, 457, publisher: Institute of Mathematical Statistics

Ginsburg, A., Sipocz, B., Madhura Parikh, et al. 2018, Astropy/Astroquery: V0.3.7 Release

Hoffman, M. D., & Gelman, A. 2014, Journal of Machine Learning Research, 15, 1593

Hunter, J. D. 2007, Computing in Science & Engineering, 9, 90

Jenkins, J. M., Twicken, J. D., McCauliff, S., et al. 2016, Software and Cyberinfrastructure for Astronomy IV, 9913, 99133E

Jones, E., Oliphant, T., Peterson, P., et al. 2001, Open source scientific tools for Python

Kipping, D. M. 2013, mnras, 435, 2152

Lightkurve Collaboration, Cardoso, J. V. d. M., Hedges, C., et al. 2018, Lightkurve: Kepler and TESS time series analysis in Python, Astrophysics Source Code Library, ascl:1812.013

Lomb, N. R. 1976, Astrophysics and Space Science, 39, 447

Luger, R., Agol, E., Foreman-Mackey, D., et al. 2019, aj, 157, 64

McKinney, W. 2010, in Proceedings of the 9th Python in Science Conference, ed. S. van der Walt & J. Millman, 51

Onitsuka, M., Fukui, A., Narita, N., et al. 2017, Publications of the Astronomical Society of Japan, 69

Paxton, B., Bildsten, L., Dotter, A., et al. 2011, ApJS, 192, 3

Paxton, B., Cantiello, M., Arras, P., et al. 2013, ApJS, 208, 4

Paxton, B., Marchant, P., Schwab, J., et al. 2015, ApJS, 220, 15

Pérez, F., & Granger, B. E. 2007, Computing in Science and Engineering, 9, 21

Raetz, S., Schmidt, T. O. B., Czesla, S., et al. 2016, Monthly Notices of the Royal Astronomical Society, 460, 2834

Salvatier, J., Wieckiâ, T. V., & Fonnesbeck, C. 2016, PyMC3: Python probabilistic programming framework

Scargle, J. D. 1982, The Astrophysical Journal, 263, 835

Smith, J. C., Morris, R. L., Jenkins, J. M., et al. 2017a, Kepler Science Document, 7

Smith, J. C., Stumpe, M. C., Jenkins, J. M., et al. 2017b, Kepler Science Document, 8

Stassun, K. G., Oelkers, R. J., Pepper, J., et al. 2018, AJ, 156, 102

Stassun, K. G., Oelkers, R. J., Paegert, M., et al. 2019, arXiv:1905.10694 [astro-ph], arXiv: 1905.10694

Tanimoto, Y., Yamashita, T., Ui, T., et al. 2020, PASJ, arXiv:2001.00148 [astro-ph.EP]

Tenenbaum, P., & Jenkins, J. 2018, TESS Science Data Products Description Document, EXP-TESS-ARC-ICD-0014 Rev D, https://archive.stsci.edu/missions/tess/doc/EXP-TESS-ARC-ICD-TM-0014.pdf

Theano Development Team. 2016, arXiv e-prints, abs/1605.02688

van Eyken, J. C., Ciardi, D. R., von Braun, K., et al. 2012, The Astrophysical Journal, 755, 42

VanderPlas, J. T., & Ivezić, Z. 2015, The Astrophysical Journal, 812, 18

Walt, S. v. d., Colbert, S. C., & Varoquaux, G. 2011, Computing in Science & Engineering, 13, 22

Yu, L., Winn, J. N., Gillon, M., et al. 2015, The Astrophysical Journal, 812, 48